FORSCHUNGSZENTRUM
ROSSENDORF e.V.

FZR

FZR-53
August 1994

O.W.M. Stins

A Retarding Field Energy Analyser to measure the Energy Distributions of Liquid Metal Ion Sources

Forschungszentrum Rossendorf e.V.
Postfach 51 01 19 · D-01314 Dresden
Bundesrepublik Deutschland
Telefon (0351) 591 3445 / 591 2866

A Retarding Field Energy Analyser to measure the Energy Distributions of Liquid Metal Ion Sources

O.W.M. Stins

University of Twente, the Netherlands

Supervisor: Dr. J. Teichert

Research Center Rossendorf Inc.

Institute of Ion Beam Physics and Materials Research

Table of Contents

Preface

My practical training at Forschungszentrum Rossendorf e.V., during 04.04.1994-15.07.1994, led to the writing of the following paper. I hope the paper will give an useful insight in the installation and testing of a retarding field energy analyser to measure the energy distributions of liquid metal ion sources and other charged particle sources.

I want to thank the group of the IMSA labour for their help and cooperation. Especially Dr. J. Teichert, to give me the opportunity to work in the IMSA labour and for useful discussions, and E. Hesse, who helped me doing the experiments and prepared the sources.

O.W.M. Stins, 07.17.1994

Chapter 1. Introduction

The liquid metal ion source (LMIS) is a device capable of producing an extremely bright beam of positive ions (~$1*10^6$ A/cm^{2}sr) [2]. Therefore the LMIS is an extensively used source for focused ion beam applications, like implantation and lithography. Because of the chromatic aberrations of electrostatic lenses, used in focused ion beam systems, the energy distribution of the LMIS becomes an important feature in their operation. Also energy distribution measurements are useful to understand the ion emission processes, because the energy distribution of the ions results from them. To measure the energy distribution of ions emitted by a LMIS a retarding field energy analyser can be used [7]. Ions with an energy high enough to pass the retarding field will be measured by a target electrode. By variation of the retarding potential an integral spectrum of the LMIS energy distribution will be obtained.

In this paper the setup and use of a retarding field energy analyser to measure the energy distribution of LMIS will be presented. An introduction in the technology and mechanism of LMIS will be given in chapter 2. The experimental configuration of the retarding field energy analyser, together with an error estimation and a computer program, to control the energy analyser and to calculate the energy distribution, will be discussed in chapter 3. To test the energy analyser an electron source, consisting of a tungsten thermoionic cathode, will be used. Energy distribution measurements of a gallium LMIS will be presented in chapter 4. Finally in chapter 5, the accuracy of the energy analyser and suggestions for improvement will be presented.

Chapter 2. LMIS; Technology and Mechanisms

This chapter provides a brief introduction to LMIS technology (§2.1) and theory (§2.2). The energy distribution of LMIS, our main point of interest, will be treated more extensively in §2.3.

§2.1 Technical Configuration

The first source configuration to be used as a liquid metal ion emitter consisted of a capillary filled with a liquid metal. Today needle emitters are mostly used, because needles are easier to operate and their stability especially at low currents (below ~10 μA) is much better then for capillaries.

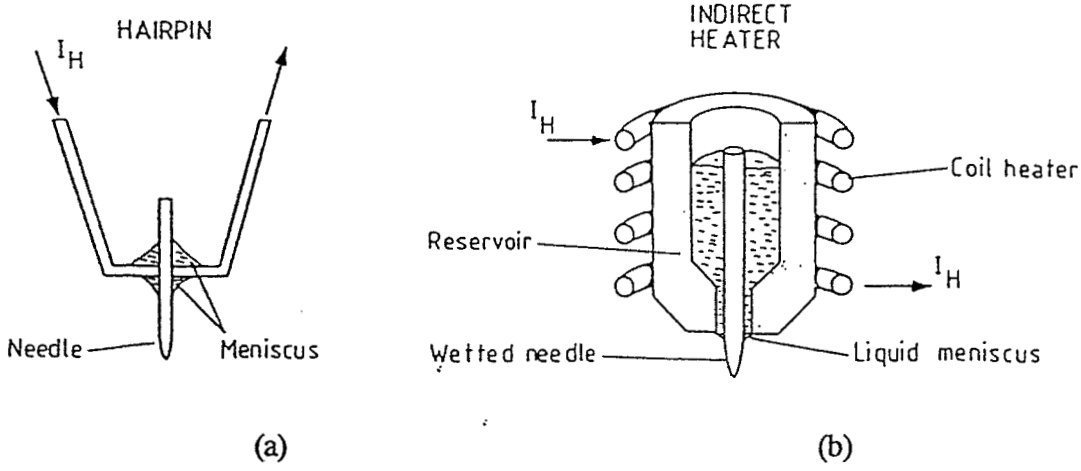

Fig. 2.1a Two different forms of needle LMIS: (a) hairpin filament source, (b) Culham type [1].

There are two different constructions of a needle type LMIS:

1. directly heated sources and
2. indirectly heated sources.

Directly heated sources are heated by a current which flows directly through the construction. The most frequently used construction of this type is the "hairpin" source, see Fig. 2.1a. The source consists of a needle which is welded on a wire that carries the heating current. The liquid metal is concentrated at the cross formed by the needle and heater loop to form a meniscus maintained

surface tension and adhesive forces.

An indirectly heated source provides for a separation of the needle and heater. The liquid metal is normally kept in a reservoir surrounding the needle and the heater is formed by a coil of wire. Sources of this type are called "Culham" sources, after UKAEA Culham Laboratory, see Fig. 2.1b. Though the Culham source allows more freedom regarding construction materials the simple hairpin source is mostly used.

The needles are produced by electrochemical etching or are mechanical formed. For electrochemical etching solutions of NaOH or KOH are used. The needle can be etched to a paraboloidal or cusp-like end form [8]. It is important that the needle is grooved along its shank and has a certain degree of roughness. Otherwise, in case of a smooth needle surface, the flow of liquid to the needle top will be restricted and the current will be limited. From further importance is the wetting of the needle. The liquid metal should wet the needle surface but not react strongly with it. This is to avoid destroying of the emitting needle.

§2.2 Basic Principles & Mechanisms

In the first paragraph, §2.2.1, the principle operation of a LMIS will be treated. In the second paragraph, §2.2.2, something will be said about the parameters of a LMIS.

§2.2.1 Operation of a LMIS

The operation of a LMIS depends on the balance between the electrical field, due to the voltage applied between the needle and the extracting counter electrode, and the surface tension of the liquid metal on the needle. The condition for surface deformation is that the electrical stress (σ_e) exceeds the stress due to surface tension (σ_s):

$$\sigma_e \geq \sigma_s \tag{1}$$

$$\sigma_e = \frac{1}{2}\epsilon_o E_0^2 \tag{2}$$

$$\sigma_s = 2\gamma / r_t \tag{3}$$

where γ is the surface tension of the liquid metal and r_t is the radius of curvature at the needle tip.

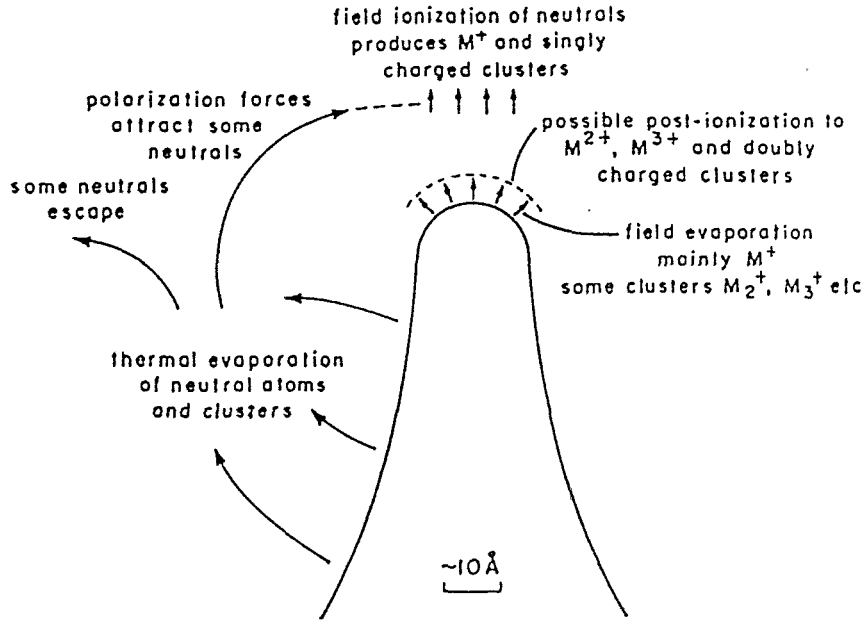

Fig. 2.2 Processes of LMIS operation around the needle tip [2].

In Fig. 2.2 the various processes of LMIS operation are pictured. Here I want to mention the three most important ionization processes: 1. field evaporation,

2. post ionization and

3. field ionization.

Field evaporation is believed to be the main ionization process. Field evaporation is the process during which a neutral atom adsorbed on a metal surface is detached from it as a positive ion under the influence of a high electric field. Post ionization is, simply said, the process during which a single charged ion by the high electric field is ionized to a n-charged ion ($n>1$). The process during which evaporated neutrals from the liquid metal surface become ionized, in free space, is called field ionization.

The surface deformation when applying an electric field to a liquid metal will form a liquid cone on top of the needle apex. Taylor [9] derived that the only possible electric field which can exist in equilibrium with a conical fluid surface is that external to a cone of base angle 49.3° [8]. As was mentioned before: field evaporation is the main ionization process in a LMIS. In order to have field evaporation there should be an electric field in the order of several tens of V/nm [1,10].

The first field calculations for LMIS where based on a Taylor cone with a rounded apex. They showed, that it is impossible to reach the required field strength for a rounded Taylor cone: A small emission area entails a high concentration of space charge, with resultant reduction in apex field. Thatswhy a jet-like elongation in front of the rounded apex region of the Taylor cone should exist [1]. Indeed, the observed film deformation of a needle LMIS is a Taylor cone with a jet-like elongation.

§2.2.2. Parameters of a LMIS

In this paragraph the following parameters of a LMIS will be discussed: current-voltage curves, mass spectra and secondary electrons. The parameter of our interest; the energy distribution will be considered separately in §2.3.

§2.2.2.1. Current-voltage curves

If a potential is applied between the needle and the extracting electrode, at distance h, the apex electric field approximates to

$$E_0 = \frac{2V_0}{r_t \ln(2h/r_t)} \tag{4}$$

Together with equations (1) to (4) the critical starting voltage, V_{oc}, for film deformation becomes

$$V_{oc} = \ln(2h/r_t)\sqrt{\gamma r_t/\epsilon_0} \tag{5}$$

The minimum value of the potential, applied between needle and extractor, for which the liquid metal cone can be sustained is called the extinction voltage, V_{ox}. The voltage needed to form the cone is somewhat higher than the voltage to sustain the cone. The difference between V_{oc} and V_{ox} is generally smaller than 10%.

The following equation

$$i = 3\pi r_t \gamma \cos\theta (2e/M)^{\frac{1}{2}} (V_o/V_{ox} - 1) V_{ox}^{\frac{1}{2}} \tag{6}$$

where θ is 90° minus the base angle of the liquid cone (49.3° according to Taylor) and e/M is the charge to mass ratio (for single charged ions), predicts the current-voltage curve. The equation, originally derived for capillaries, appears to be a good approximation for needle LMIS, see

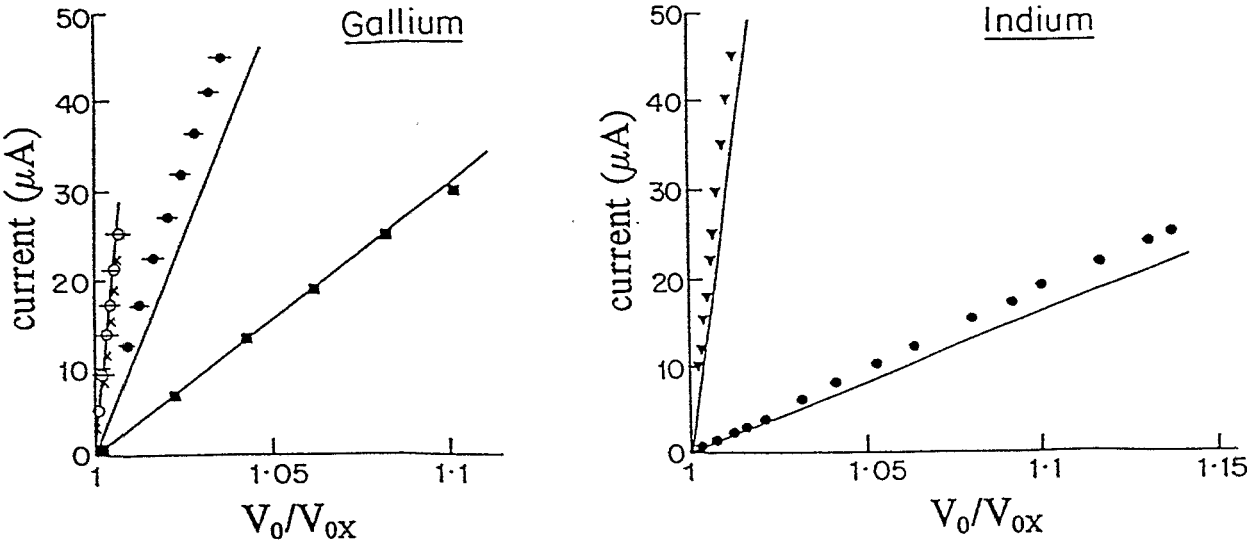

Fig. 2.3. Comparison of normalized curves with theory, equation (6) [1].

Fig. 2.3. The good approximation can be understood by noticing that most needle LMIS have low flow impedances like capillaries. In case of needles with high flow impedance, for example smooth needles, the flow of liquid metal to the needle apex is limited. Therefore, the current-voltage curves of those needles cannot be approximated by equation (6).

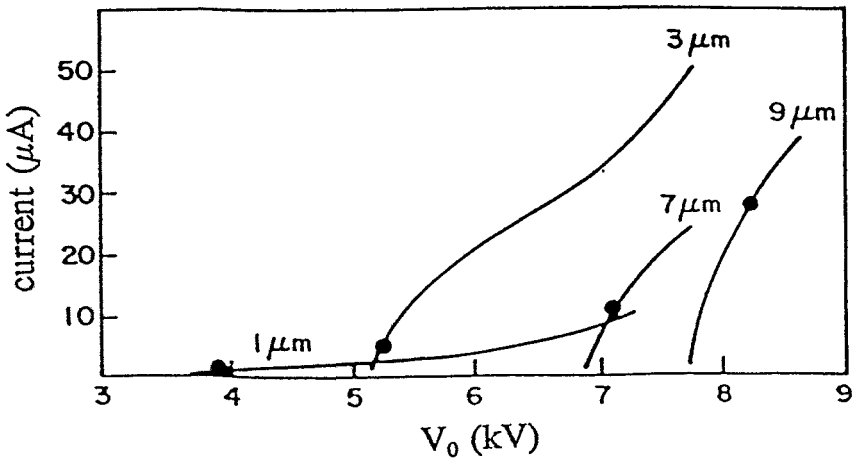

Fig. 2.4 Current-voltage characteristics for gold ion sources of varying needle radii [1].

The flow impedance decreases with increasing radius of curvature at the needle tip and with the roughness of the needle surface. The lower the flow impedance the steeper the current-voltage curves. Fig. 2.4 shows the dependence of the current-voltage curve on the needle radii.

§2.2.2.2. Mass spectra

Ion beams emitted from LMIS have a variety of ionic species. The charge to mass ratio and other parameters, like the energy spread, hint to the emission mechanisms. The principal species for most LMIS are M^+ formed by field evaporation. This is especially true for metals with light atomic masses. For example an ion beam emitted from a gallium LMIS consists of ≈99.9% Ga^+ [11].

§2.2.2.3 Secondary Electrons

Secondary electrons in a LMIS system can be released from every electrode touched by the beam. The following discussion holds for an arrangement consisting of the ion source and a collector. By adding to the measured ion current, up to ≈50%, secondary electrons cause for difficulties in evaluating data between different researchers. To avoid adding of secondary electrons to the measured ion current it is enough to suppress the collector released secondary electrons. Collector released secondary electrons can be suppressed by applying external electric or magnetic fields.

§2.3 Energy Distribution

An ion beam emitted from a LMIS consists of neutrals and a lot of different ionic species, each with its own energy distribution. The energy distribution of one kind of ions consists of one or more Gaussian-like functions, with different energies for their peak values, called peak energy deficits (PED). It is believed that only processes in the ion source contribute significantly to the energy distribution. The processes which occur in the ion source and are of importance for the energy distribution are the ionization processes and the ion-ion Coulomb interactions. In the following two paragraphs the energy deficit (§2.3.1) and the energy spread (§2.3.2) will be discussed.

§2.3.1 Energy Deficit

In LMIS the ions are created at some distance from the liquid surface. Therefore the ions are accelerated by a smaller accelerating voltage than is applied between emitter and extractor. The difference is called energy deficit. The theoretical value, called critical energy deficit, for the energy deficit for field evaporation is the expended work needed to create a free ion by detaching an atom bound on the surface of the emitter in the presence of an electric field.

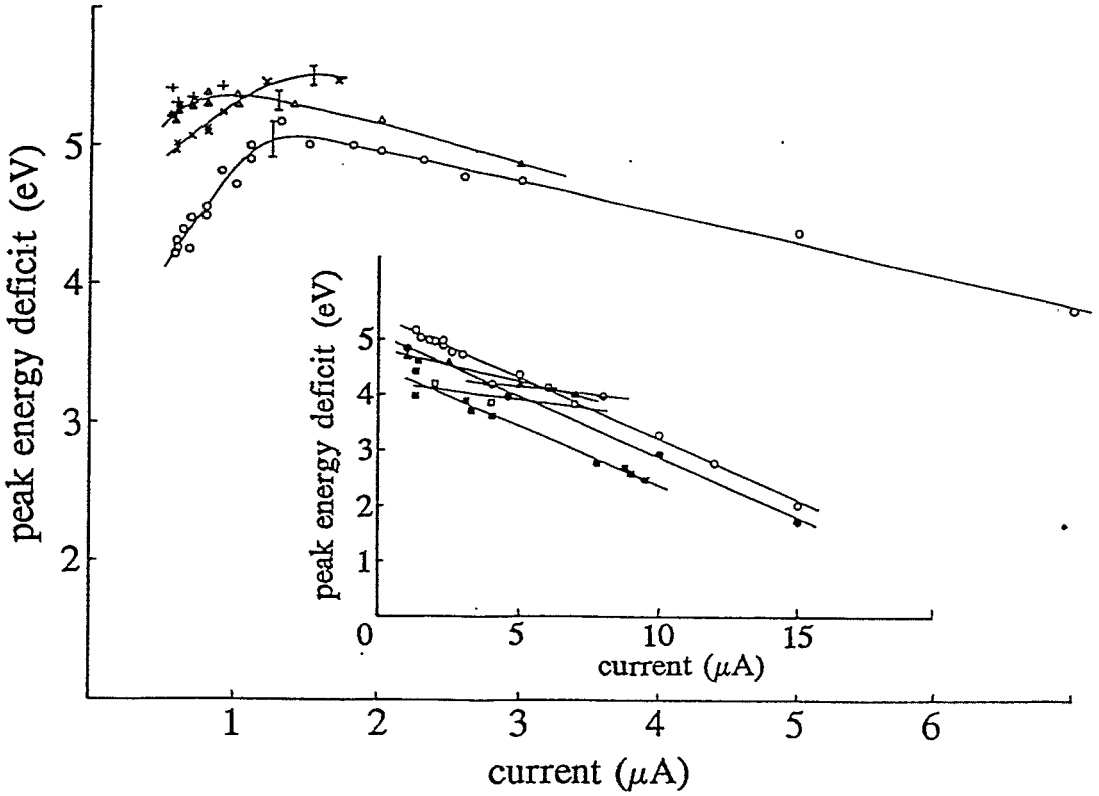

Fig. 2.5 Peak energy deficit of Ga^+ energy distribution [12].

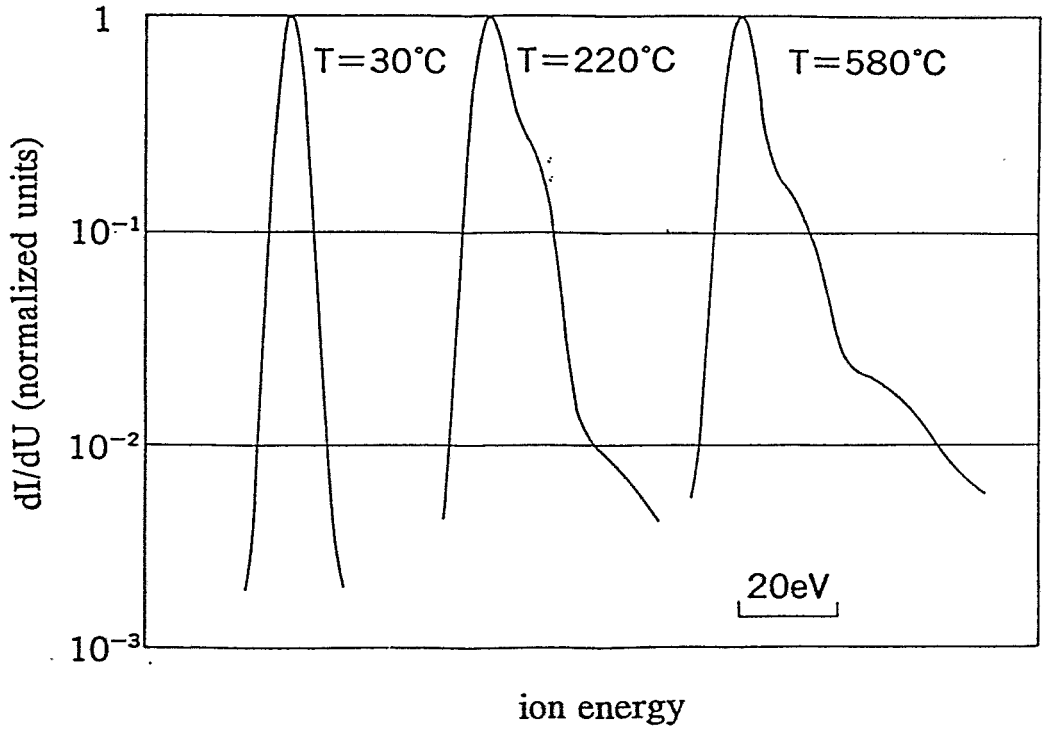

Fig. 2.6 Temperature dependence of energy distribution for Ga LMIS at 1 μA [13].

The critical energy deficit can be calculated with:

$$\Delta E_c = \Lambda + \Sigma_n I_n - n\phi_c - Q \qquad (7)$$

where: Λ - is the heat of evaporation of the surface atom (subsequently ion),

I_n - is the n^{th} ionisation potential of the surface atom,

Φ_c - is the work function of the retarding electrode,

n - is the ion charge and

Q - is the field-dependent activation energy for field evaporation.

The work function of the retarding electrode can be estimated by measuring the energy deficit of an electron source and calculating the work function of the grid with the following equation:

$$\phi_c = \phi_n + \frac{3}{2}kT_e - E_d \qquad (8)$$

where: ϕ_n - is the workfunction of the electron sources needle material (=4.53 eV when using a tungsten needle [5]),

k - is the Boltzmann constant,

T_e - is the temperature of the emitting needle and

E_d - is the measured energy deficit of the electron source.

Fig. 2.5 shows the peak energy deficit (PED) versus source emission current for Ga^+ emitted from a gallium LMIS. For currents in excess of 2 μA the PED decreases linear with increasing current. A possible explanation may be the following: An increasing current means an increasing number of emitted ions and the space charge directly in front of the needle tip will increase. Therefore the distance from the needle surface where the electrical field is high enough for FE will be smaller and the PED decreases. In the current region 0.5...1.5 μA the PED increases with current. Prewett and Mair [1] give the following explanation: Assume that the ion-ion Coulomb interactions in this current range are negligible. Then the heat of evaporation will increase with increasing electric field and the energy barrier seen by an escaping ion will decrease. This would increase the PED consistent with equation (7).

Fig. 2.5 shows fluctuations between different PED measurements done with retarding field energy analysers. According to Mair [12] the fluctuations in PED measurements are due to contaminations of the retarding electrode, which change the work function of the retarding

electrode. From Fig. 2.5 one can see that the energy deficit is in the order of electron volts. This suggests, that the main ionization process is field evaporation. Field ionization would have shown energy deficits in the order of a few tens of eV (for Ga^+ it is ~10 eV). Because field ionization takes places in free space while field evaporation occurs at a distance of 0.1 nm from the apex of the elongation of the liquid cone, the PED for field ionization is larger.

Fig. 2.6 shows the temperature dependence of the Ga^+ energy distribution. For higher temperatures two additional peaks seem to occur. The highest peak has the least PED and is due to field evaporation. The second peak has a PED of 9 eV as expected for the field ionization process. The third peak, at 34 eV, is assumed to be due to a charge transfer process between neutrals and single charged ions [13].

§2.3.2 Energy Spread

The energy spread is normally expressed in terms of the full width at half maximum (FWHM). Fig. 2.7 show the FWHM of M^+ and M^{2+} of various LMIS. As can be seen the energy spread is a monotonically increasing function of the emission current. The increase of the FWHM with current is caused by ion-ion Coulomb interactions. The same interactions cause for an increase in FWHM with increasing ion mass and with increasing ion charge.

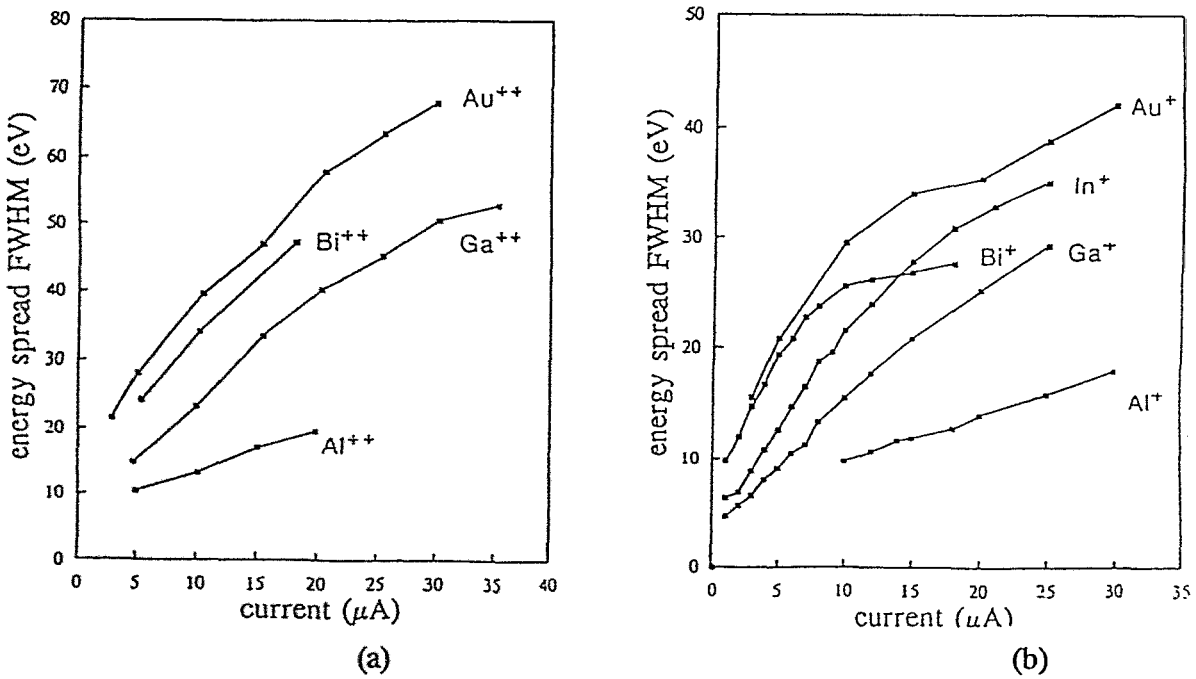

Fig. 2.7 The FWHM for the M^+ , (a), and M^{2+} species, (b), of various LMIS as a function of emitted current [11].

Knauer [1] predicted a 2/3 power dependence of FWHM with current:

$$\Delta E_{1/2} = \frac{5.8\pi e}{4\pi\epsilon_0}(M/V_0)^{1/3} R_s^{1/3} \left[\frac{i}{2\pi(1-\cos\alpha)}\right]^{2/3} \qquad (9)$$

R_s is the effective source size, V_0 the beam potential and α the half-angle beam aperture; e and M are respectively the ion charge and mass. Knauer assumed collisionless Coulomb interactions near the surface of the emitter. The formula is in good agreement with the FWMH for Ga^+ in the current region of 2...25 μA. But other measurements can not be described with the formula.

Fig. 2.8 shows a logarithmic plot of the Ga^+ FWHM versus emission current. The curve can be devided in three parts:

1. for currents < 2μA; the FWHM will never be below 5eV [11],
2. for currents = 2...25μA; in this part the energy broadening is mainly caused by non-collisional ion-ion Coulomb interactions.
3. for currents > 25μA; here the broadening is due to non-collisional and collisional ion-ion Coulomb interactions both.

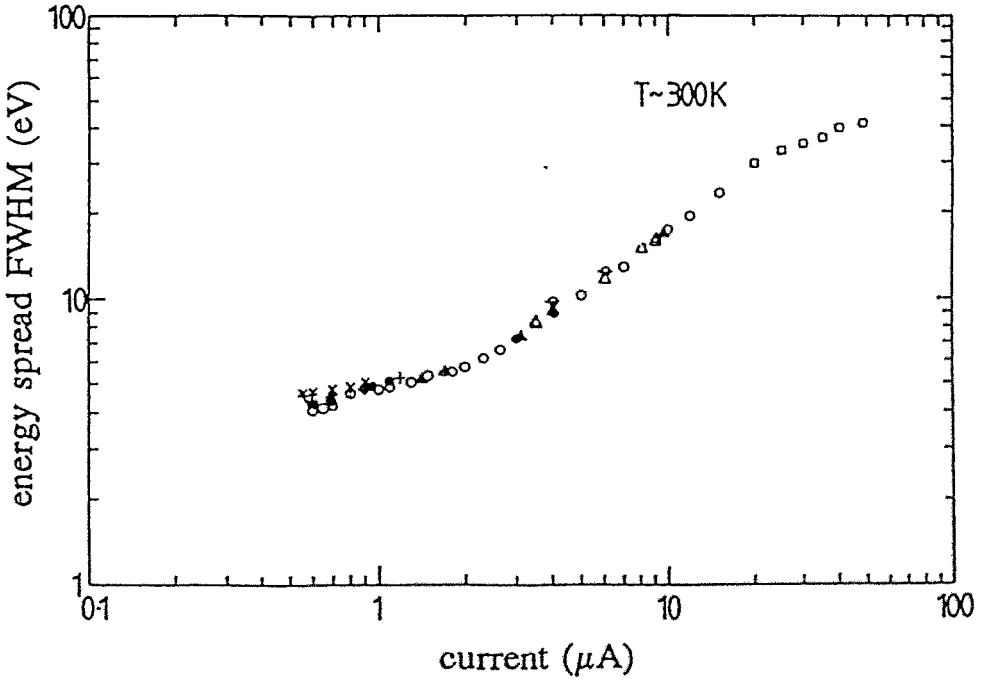

Fig. 2.8 Logarithmic plot of the Ga^+ FWHM vs. emission current [1].

Fig. 2.9 shows FWHM of Ga^+ vs emission current. As one can see there the FWHM increases with increasing temperature. This behaviour could be explained by a larger number of field ionized ions with increasing temperature.

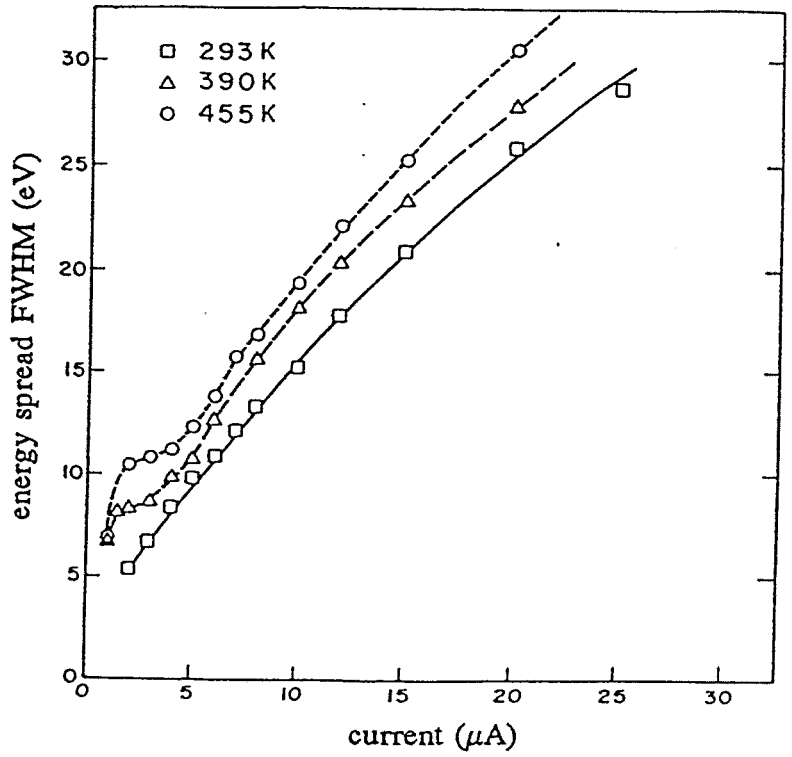

Fig. 2.9 FWHM for Ga^+ versus emission current for different operating temperatures of the gallium LMIS [1].

Chapter 3. Experimental Setup

The experimental setup of the retarding field energy analyser will be discussed in the following chapter. The technical configuration will be described in §3.1 and the error estimation, depending on the apparatus and adjustment, is discussed in §3.2. To operate the energy analyser a computer program has been written, see §3.3.

§3.1 Technical Configuration of the Retarding Field Energy Analyser

The actual measurement tube will be described in §3.1.1 and the electronics in §3.1.2.

§3.1.1 The Measurement Tube

The Retarding Field Analyzer is enclosed in a tube to prevent any influences of scattered particles from the outside. The tube is mounted in a vacuum system. The used pumps are a turbo-molecular pump and a rotary-vane vacuum pump [4]. The system allows working pressures of ~$1*10^{-6}$ Torr. The configuration of the measurement tube and ion source is shown in Fig. 3.1. The retarding field analyser consists out of three parts:

1. the collimator,
2. double grid, and
3. a secondary electron multiplier.

1. The Collimator.

The collimator extracts a small part of the beam and is formed by two apertures; the first with a diameter of 0.42 mm and the second with a diameter of 0.60 mm. In order to create a nearly homogenous electric field between the second aperture of the collimator and the retarding electrode, a grid is spread across the second collimator aperture. The grid has a transmission coefficient of 0.22 and is made of copper wires with a golden surface.

2. The Double Grid.

A double grid is used as a retarding electrode. The double grid consists of two grids, 0.7 mm seperated and made out of copper wires with a golden surface. The square meshes have a hole size of 105 μm and the wires are 30 μm thick.

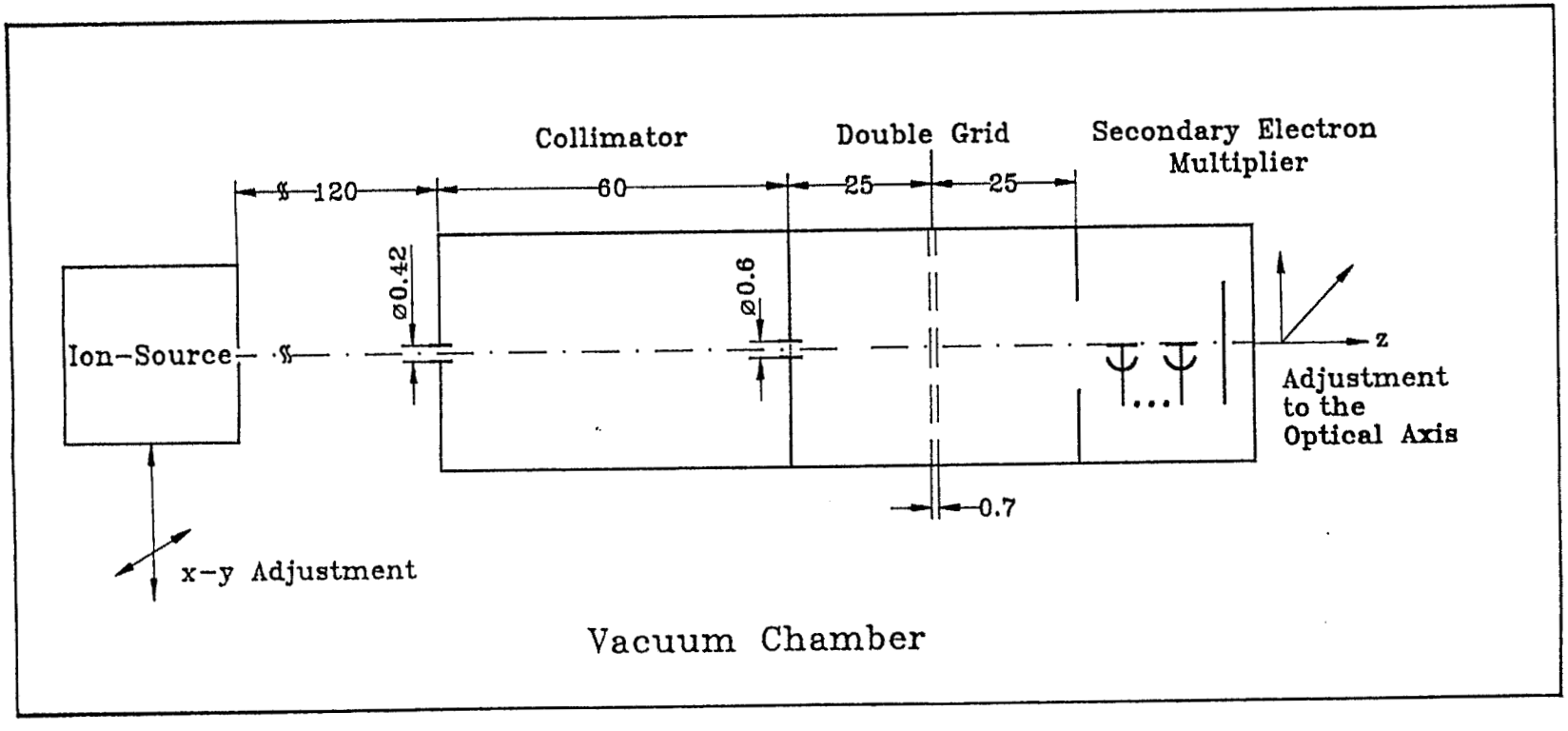

Fig. 3.1 The measurement tube.

3. The Secondary Electron Multiplier.

A secondary electron multiplier amplifies the ion current signal. The maximal amplification factor of the secondary electron multiplier is 10^7 and the voltage needed for maximal gain is ~3kV.

The measurement tube can be adjusted to the optical axis and additionally the ion source can be x-y adjusted. It was found that the secondary electrons, released from the surface of the measurement tube, have no influence on the measured emission current of the source. Therefore it was not necessary to apply a suppression voltage to the collimator.

§3.1.2 Electronic Equipment

Fig. 3.2 shows the set up of the retarding field energy analyser. The purpose of the electronic equipment is to control the ion source, to apply a grid potential and to measure the ion current that is able to transfer through the grid. The used devices are:

- Heating; to heat the ion source with currents up to 10A,
- Controlling-personal computer Schneider PC1512,
- 8-16 Bit A/D-D/A-converter ADA16 in the personal computer,
- Secondary electron multiplier; to amplify the ion current,
- Current measurement device MV40 ; to measure the amplified ion current,
- Isolationamplifier (1:1); for ground potential separation between the MV40 and the ADA16,
- DC-Driver; to apply the grid potential in the range of ± 30 V based on the emitter potential
- Optocoupler; between the DC-Driver and the ADA16,
- High voltage equipment.

The computer controls the grid potential, via the DC-Driver with a resolution <0.02 V. The MV40 measures the output of the secondary electron multiplier, the amplified ion current signal. The output voltage of the MV40 being proportional to the measured current is applied to the ADA16. The resolution of current measurement is given by: (the maximum value of the measurement range of the MV40)/2048. To obtain the energy distribution the measured current is derived with respect to the applied retarding potential by a computer program, see §3.3.

The arrangement used for measurements in this paper differs from the arrangement described above. The grid potential was applied by a separate high voltage device instead of using the emitter

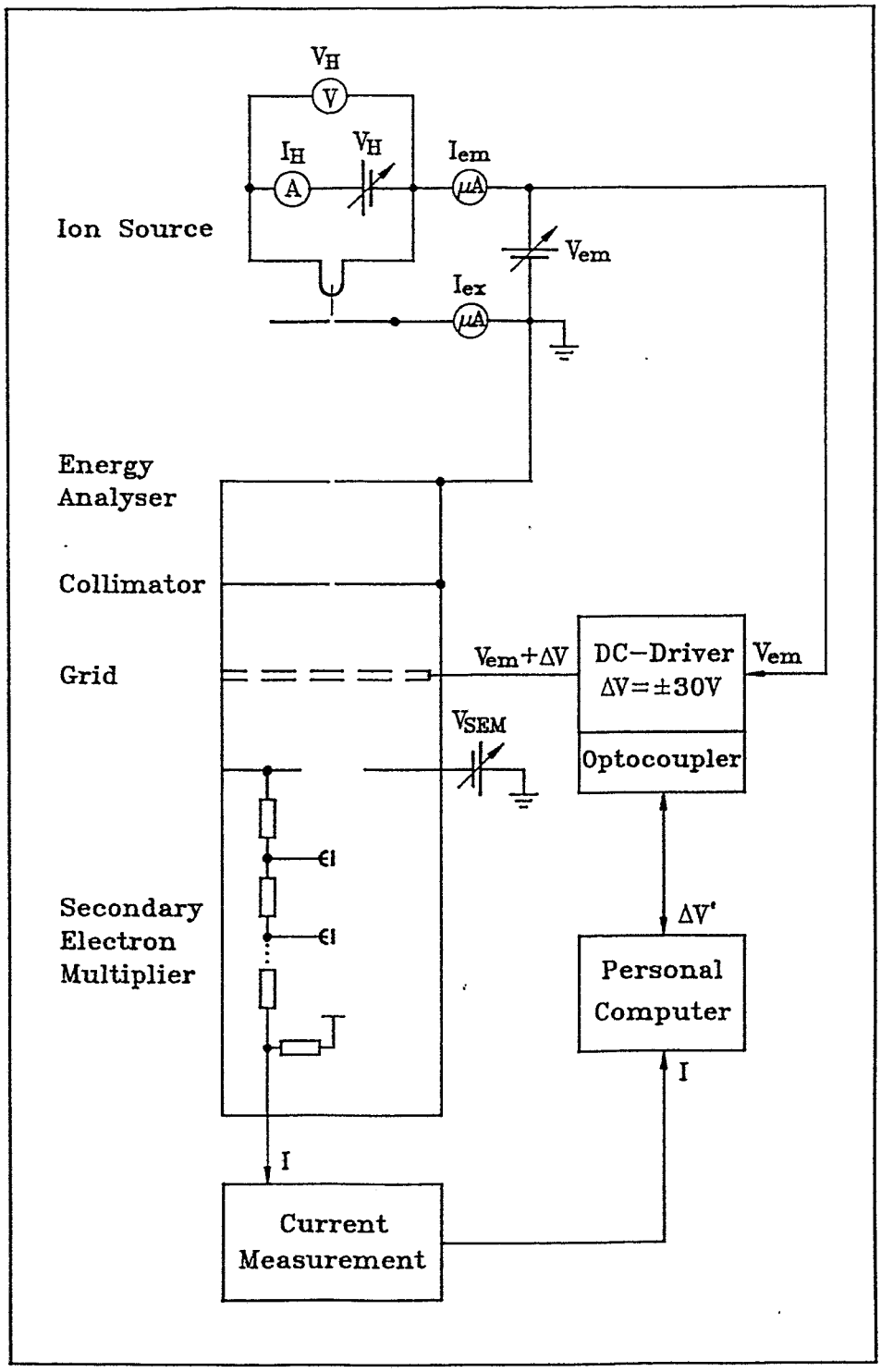

Fig. 3.2 The set up for a retarding field energy analyser, the grid potential is based on the emitter potential.

V - voltage, I - current, H - heating, em - emitter, ex - extractor,

SEM - secondary electron multiplier,

voltage in combination with a DC-Driver. The difference in this set up has two disadvantages:

1. there is additional electrical noise introduced and
2. it is impossible to measure energy deficits.

The separate device to apply the grid potential was controlled by a computer and it was operated in the range of 0...6000 V, resolution <0.1 V.

§3.2 Error Analyses

In §3.2.1 the apparatus error of the retarding field analyser will be estimated [14]. The adjustment error will be discussed in §3.2.2.

§3.2.1 Apparatus Error

The resolution of the retarding field analyser is mainly defined by the angle of the particles to the retarding electrical field lines, and the decrease of grid potential in the grid meshes. So these two parameters define the apparatus error, ΔE, of the energy spread and the difference, ΔE_p, to the most probable energy.

The electrical field retards the axial velocity component of the particles only. So particles with an angle α to the field lines will be retarded earlier with:

$$\Delta E_\alpha = \sin^2\alpha \sim \alpha^2 \qquad (10)$$

The angle, $\alpha=\alpha_1+\alpha_2$, is for one part, α_1, determined by the aperture radius r_{C2} of the second collimator filter, its distance l to the source and the radius of the emitting source size. The radius of the emitting source size is in the order of several tens of nanometers and will be neglected. So α_1 becomes $\alpha_1=r_{C2}/l$. The difference in the electrical field magnitude on both sides of the second collimator aperture has a diverging effect on the beam. This causes a second contribution to α of $\alpha_2=r_{C2}/4d$ [14], where d is the distance between the second collimator aperture and the grid. Altogether it becomes:

$$\frac{\Delta E_\alpha}{E_o} = \left(\frac{r_{C2}}{l}+\frac{r_{C2}}{4d}\right)^2 \sim 2.18\cdot 10^{-5} \qquad (11)$$

The radial potential decrease $\Delta\Phi$ of the grid potential inside a grid mesh gives rise to a second error ΔE_A. Sakai [15] derived the following equation:

$$\frac{\Delta E_A}{E_0}=\frac{\Delta\Phi}{U}=\frac{r_M}{\pi d}\left[1+\frac{D}{r_M}\arctan\left(\frac{D}{2r_M}\right)-\frac{D}{r_M}\arctan\left(\frac{D}{r_M}\right)\right]\approx 1.24\cdot 10^{-5} \qquad (12)$$

where $r_M=0.565g$ (replacement of the square grid hole with meshside g by a circular aperture of the same size) and D the distance between both grids of the double grid [14].

Particles with an energy E_0, are faded out by the grid for grid potentials $U \ll U_0$. But these particles will be focused through the grid meshes for grid potentials $U \leq U_0$ and give rise to an additional current for retarding potentials smaller than U_0. This causes a third part of ΔE:

$$\frac{\Delta E_F}{E_0}=\frac{D}{2r_M}\left(1+\frac{D}{4r_M}\right)\frac{\Delta\Phi}{U}\approx 0.35\cdot 10^{-5} \qquad (13)$$

where D is the thickness of the grid wires, as derived by Sakai [15].

Altogether a monoenergetic beam of energy E_0 will experience a widening of

$$\frac{\Delta E}{E_0}=\frac{\Delta E_\alpha}{E_0}+\frac{\Delta E_A}{E_0}+\frac{\Delta E_F}{E_0}\approx 3.8\cdot 10^{-5} \qquad (14)$$

and have a difference of

$$\frac{\Delta E_P}{E_0}=\frac{\Delta E_A}{2E_0}-\frac{\Delta E_\alpha}{2E_0}-\frac{\Delta E_F}{2E_0}\approx -1.2\cdot 10^{-5} \qquad (15)$$

to the most probable energy.

We used the approximation of Sakai though our arrangements differ:

1. the entrance of the secondary electron multiplier is negative and not on earth potential. So the actual error, ΔE, will be larger and
2. a double grid with spacing D between both grids is assumed to be the same as one grid with width D, this makes that our grid dimensions do not agree with the ones for which Sakai derived his equations.

§3.2.2 Adjustment Error

The system is adjusted to a maximum of the secondary electron multiplier current at constant applied voltages. The measurement error dependent on adjustment is negligible, see [14]. An angle dependence of the ion energy distribution would cause an additional error. But the energy

distribution of a gallium LMIS is independent for small angles [16] and will not effect the measurement error.

§3.3 Computer Program

A computer program was written to control the grid potential and to measure the current, see §3.3.1. Data processing possibilities, like calculation of the actual energy distribution, are described in §3.3.2.

§3.3.1 Control of Grid Potential and Current Measurement

The program uses the ADA16 to control the grid potential and to measure the ion current. The both converters are used in the 12bit mode. The following pins of ADA16 are used:

PIN1 Mass,

PIN2 D/A-Canal for grid potential control and

PIN15 A/D-Canal for current measurement.

For correct current measurement the measurement ranges of computer and MV40 must be the same. The measurement range in the program can be changed using menu option "Change measurement range" or by using the keys F7 and F8. A measurement series can be done with menu option "Measurement Series". Each measurement series is stored in a data number, with a maximum of ten.

§3.3.2 Data Processing

As said before each measurement series will be stored in a data number. With menu option "Write data" it is possible to write the data in a file named: "eddat???.dat", where ??? for own use. The file can be read again with "Read data". To plot the ion current versus retarding potential for a measurement series choose option "Plot Data".

For calculation and a graphic representation of the energy distribution use option "Plot differential". A measurement series is numerically derived as follows:

$$\frac{dI}{dU}(p) = \frac{I(p+1) - I(p)}{U(p+1) - U(p)} \qquad (16)$$

$$U(p) = \frac{1}{2}[U(p+1) + U(p)] \qquad (17)$$

Thereby p is the number of the measurement within a measurement series, I is the output signal of the secondary electron multiplier, measured by the MV 40, U is the retarding potential.

Table 3.2 explains the other calculated values. To store the calculated energy distribution in a file named: "difed???.dat", where ??? for own use, use key F4.

Table 3.2 Explanation of the calculated values.

(dI/dU)max	- measured peak value
at	- retarding potential at measured peak value
dEH	- measured FWHM
PED	- statistical calculated mean value [3]
FWMH	- statistical calculated FWHM

Chapter 4. Measurements and Discussions

The test of the retarding field analyser by an electron source is described in §4.1. Energy distribution measurements, dependent on emission current and temperature, of a gallium LMIS are presented in §4.2.

§4.1. An electron source

To test the energy analyser an electron source was used. The energy distribution of an electron source is a thermal one and the FWHM is therefore $2kT_e$ [5], where k is the Boltzmann constant and T_e is the temperature of the emitting needle. The electron source is discussed in §4.1.1, the test measurements in §4.1.2 and analyses are given in §4.1.3.

§4.1.1 The Electron Source

As electron source a tungsten wire, bent to a "hair pin", was used. The temperature of the emitting area belonging to a specific heating current was visually estimated, using a colour temperature table see [6]. The applied heating currents for the electron source were around 3.0 A, what corresponds with a FWHM of around 0.35 eV.

§4.1.2 Energy Distribution Measurements

Reproducible smooth energy distributions are measured by varying the grid potential by a step size of 0.4 V. Fig. 4.1 shows an energy distribution of the electron source. The energy distributions were measured for applied emitter potentials in the range of 2.0...5.0 kV. FWHM values in the range of 1.0...1.5 eV have been measured, but no clear dependence on the extraction voltage or heating current was found. During increasing the retarding potential the current measured by the secondary electron multiplier rises before decreasing.

In order to avoid the repulsion of electrons, the energy distribution measurements have been carried out by applying only a small negative voltage to the secondary electron multiplier.

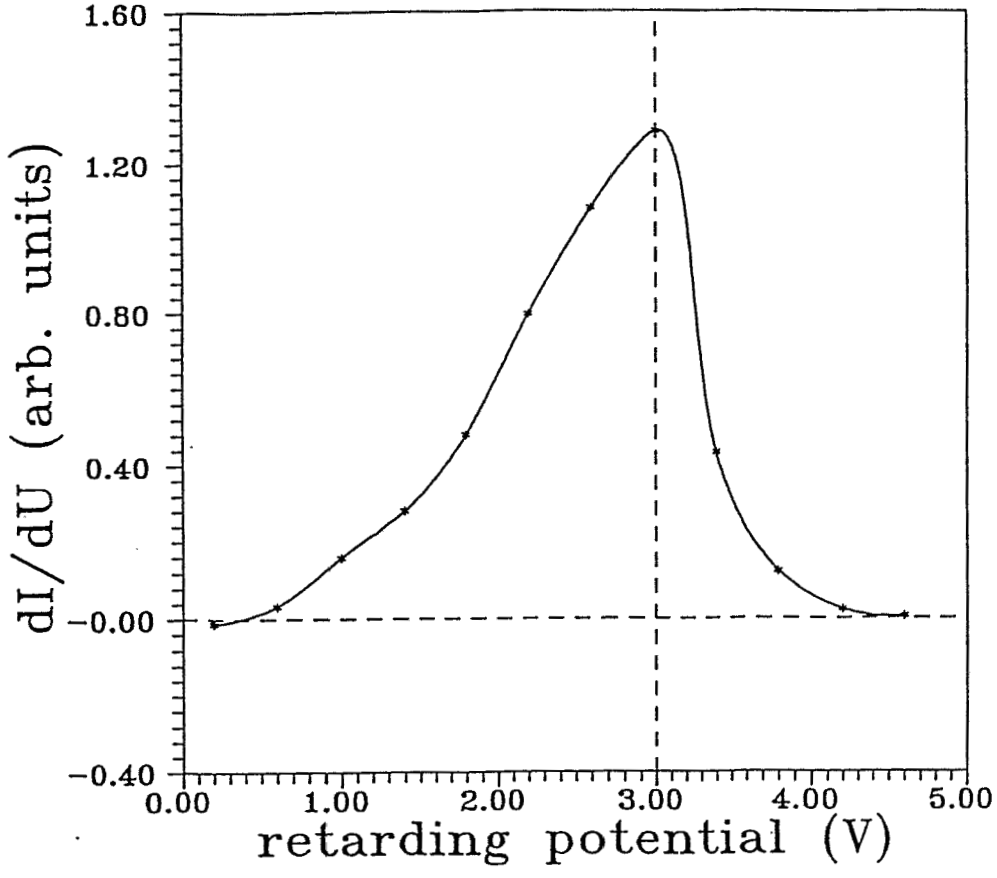

Fig. 4.1 Measured energy distribution for an electron source.

§4.1.3 Discussions

The effect that the current, as measured by the secondary electron multiplier, first increases with increasing retarding potential before it finally decreases, can be explained by an electrostatic converging lens effect of the grid. The effect makes it difficult to discuss the real form of the energy distribution curve.

The systematic error is increased by the large step size the grid potential is varied by, compared to the FWHM of around 0.35 eV of the electron source. The actual systematic error, only dependent on the measurement tube configuration may be smaller. The average measured FWHM is 1.25 eV with an accidental error of ± 0.25 eV. This leaves a systematic spreading of the FWHM, as measured by the retarding field energy analyser, of 0.7 eV.

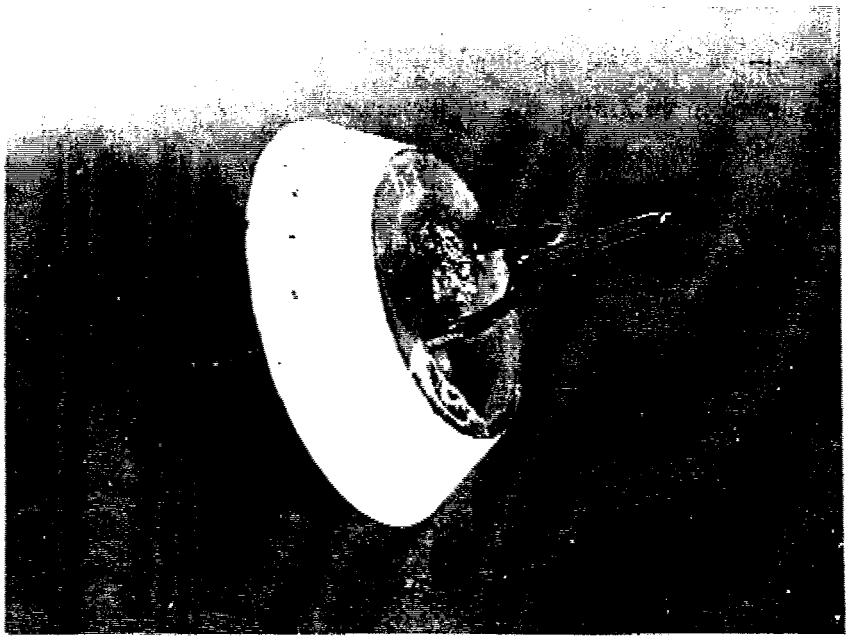

Fig. 4.2 Photograph of a "hairpin" gallium LMIS, similar to the one used in the experiment.

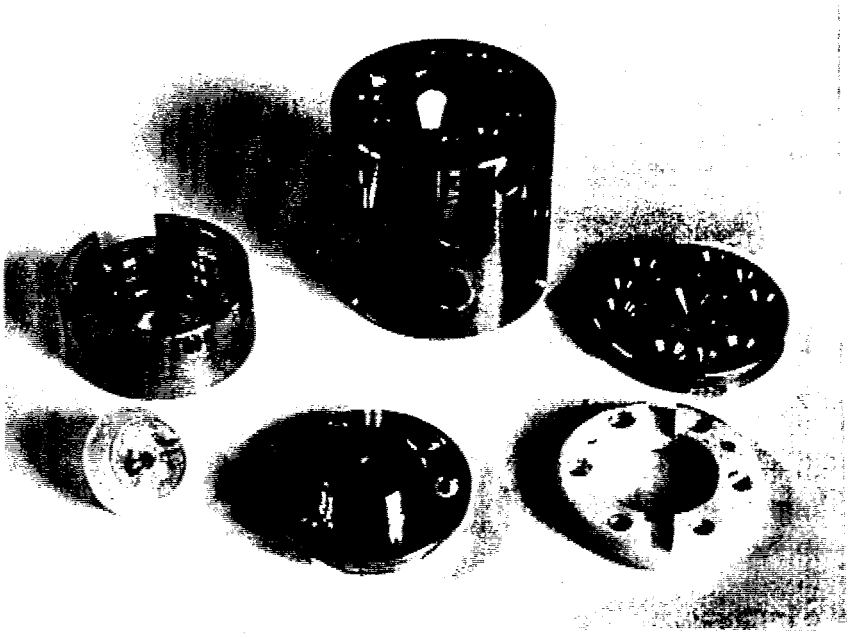

Fig. 4.3 The separate parts of the ion source construction.

§4.2 Energy Distribution Measurements of a Gallium LMIS

The used gallium LMIS is described in §4.2.1. The energy distributions of the gallium LMIS have been measured using the retarding field energy analyser, §4.2.2. The measured energy distributions are discussed in §4.2.3.

§4.2.1 The Gallium LMIS

The used gallium LMIS was a "hairpin" source, see photo in Fig. 4.2. Fig. 4.3 shows the separate parts of the ion source construction. The used emitter needle had a paraboloidal apex with a radius of curvature of ~ 4 μm. As emitter needle material tungsten was used. Fig 4.4 shows a Scanning electron micrograph of a, still unwetted, emitter needle. Especially the rough surface is very well shown.

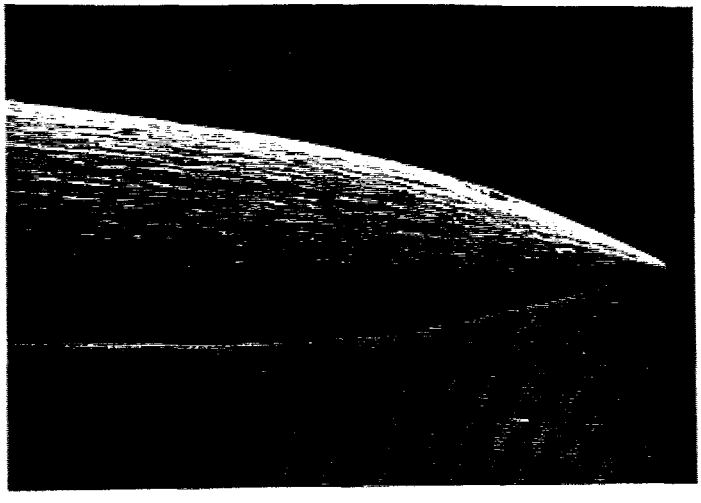

Fig. 4.4 Scanning electron micrograph of a, still unwetted, needle.

For a heating current of 2.9 A the temperature of the emitter needle was visually estimated to be about 800°C, see §4.1.1. From this values the temperature at a given heating current has been estimated using the following equation:

$$\Delta T = C * I^2 \qquad (18)$$

where: - ΔT is the temperature difference to room temperature,

- I_H is the heating current and
- C is 92.2 °C/A^2.

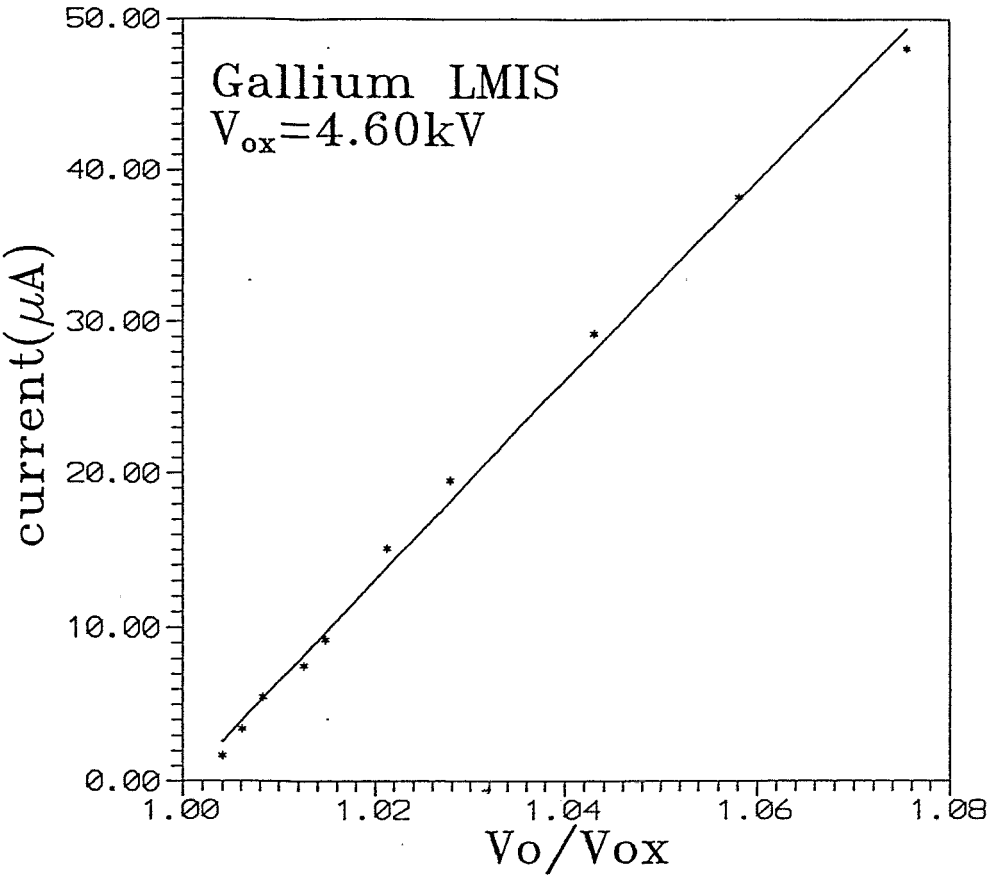

Fig. 4.5 Measured, normalized, current-voltage curve for the used gallium LMIS

Fig. 4.5 shows the measured current-voltage curve for the used gallium LMIS. According to equation (6) the linear dependence on the emission current on V_0/V_{0x} was found.

§4.2.2 Energy Distribution Measurements

Reproducible smooth energy distributions are measured by varying the grid potential by a step size of 2.0 V. Fig. 4.6 shows a retarding potential versus current curve and Fig. 4.7 a measured energy distribution curve. The energy distributions, for the gallium LMIS, are measured for emission currents in the range of 1.7...30 μA and for temperatures of 25°C, 600°C and 700°C. Because it was only possible to operate the LMIS at constant emitter voltage, instead of a current control mode, the emission current could fluctuate during the measurement. Therefore it is difficult to measure the energy distribution for large emission currents.

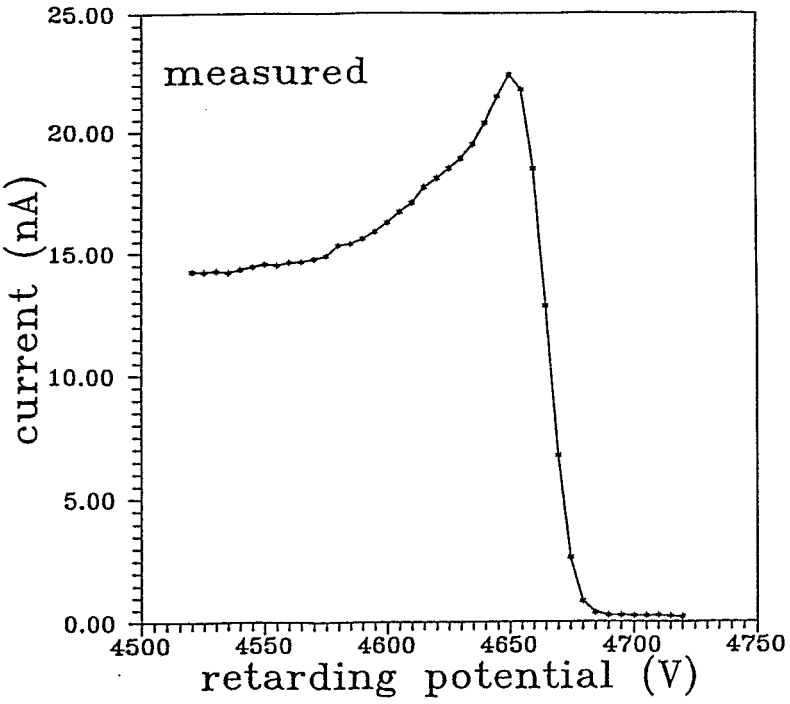

Fig 4.6 Emission current vs. retarding potential for a gallium LMIS operating at a current of 12 μA.

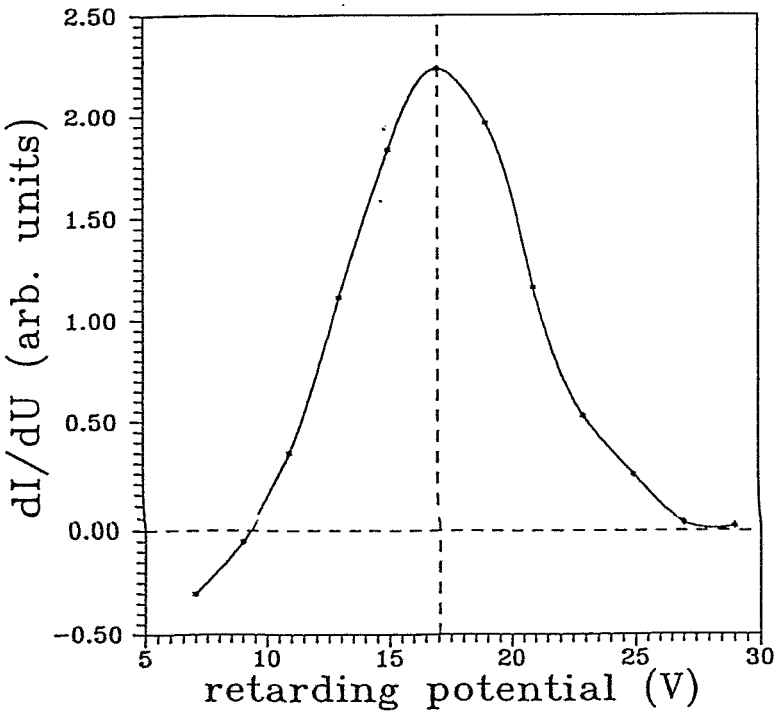

Fig. 4.7 Energy distribution for a gallium LMIS operating at a current of 3.4 μA.

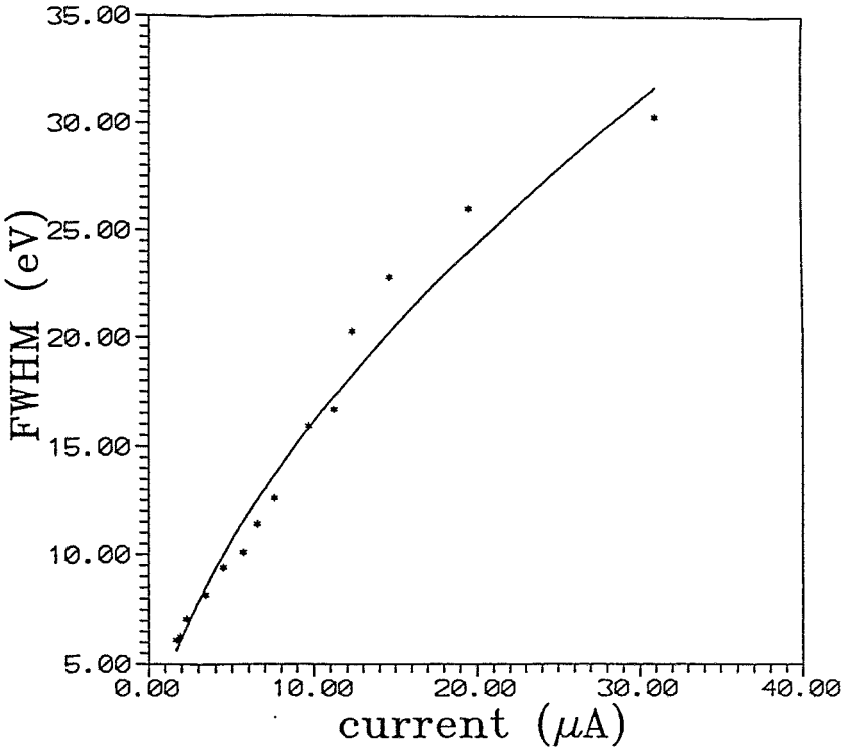

Fig. 4.8 Energy spread vs. emission current measured from energy distribution curves.

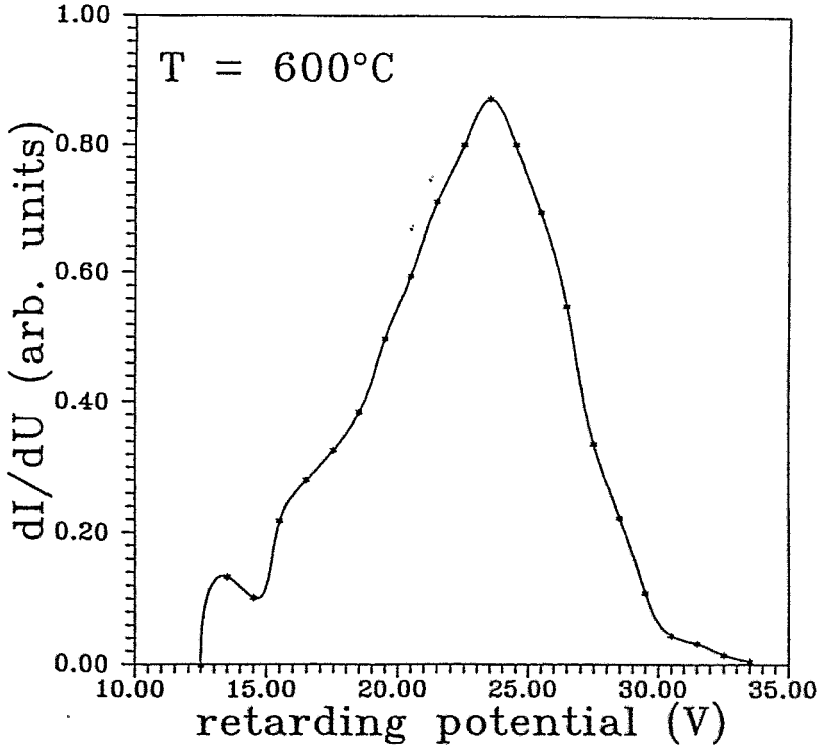

Fig. 4.9 Energy distribution for a heated gallium LMIS operating at a current of 1.7 μA.

Fig. 4.8 shows the measured FWHM versus emission current. The FWHM has as measured power dependence on the emission current of 0.59. An increase of the energy spread with increasing temperature has been measured. At higher temperatures a shoulder appears on the low energy side of the main peak, see fig. 4.9. The energy deficit measured from the main peak position is about 6 eV.

§4.2.3 Discussions

The electrostatic converging lens effect of the grid, see §4.1.3, appeared also in the energy distribution measurements for the Ga LMIS, see Fig 4.6. The ratio of measured current at low retarding potentials to maximum measured current is 0.6. This value equals the transparancy of the grid. Therefore all the particles, that should be stopped by the grid, are focused through the grid meshes.

As expected, the total energy distribution at room temperature shows one peak; due to field evaporation. The shoulder in the energy distribution can be explained as a peak due to the field ionization process. Because of the electrostatic converging lens effect of the grid it was not possible to measure a third peak, due to charge transfer.

The measured power dependence of the FWHM on the emission current of 0.59 is similar to the theoretical value of 2/3 as was derived by Knauer for non-collisional ion-ion Coulomb interactions, see equation (8). The measured FWHM values are somewhat higher as measured by Swanson [11].

Chapter 5 Summary

The retarding field energy analyser to measure the energy distribution of a LMIS has been successfully tested. To determine the energy resolution of the analyser an electron source was used. A systematic spreading of 0.8 eV of the FWHM was found. This resolution is sufficient for the measurement of energy distributions of LMIS.

Energy distributions of a gallium LMIS dependent on emission current and temperature have been measured. The measurements showed an additional error of the energy width due to the noise of the high voltage supply and the instabilities of the emission current of the ion source. For this error a value up to 1.0 V was found at emission currents lower than 10 μA. This measurement error could be reduced by applying the grid potential based on the emitter potential. A possible way for doing this has been presented in §3.1.2. Using this arrangement the electrical noise due to the high voltage equipment would be less. The current fluctuations could be reduced by operating the LMIS in a current control mode. Furthermore this arrangement would allow energy deficit measurements.

A disadvantage of retarding field analysers is the electrostatic converging lens effect of the retarding electrode. Because of this, it is difficult to discuss the shape of a measured energy distribution curve. An improvement could be made by correcting the measured energy distributions with respect to the electrostatic converging lens effect. The latter can be estimated by trajectory calculations of ions near the retarding grid. The trajectories have to be calculated for different initial energies of the ions relative to the grid. Another way to eliminate the electrostatic converging lens effect is to measure the energy distribution of an electron source. It can be observed, how the energy distribution shape differs from a Gaussian distribution [3], expected for a thermal emission process [5]. With this knowledge the electrostatic converging lens effect can be corrected.

References

1. Prewett, P.D. and Mair, G.L.R., Focused ion beams from liquid metal ion sources, Research studies press LTD, Taunton, England, 1991.
2. Brown, I.G., The physics and technology of ion sources, ed. by I. G. Brown.-Wiley & Sons, New York [u.a.], 1989
3. Burr, I.W., Applied statistical methods, Academic press, New York, 1978.
4. Görlich, P.H.C. and Schneider, H.C., Vakuumphysik und -technik, Akademische Verlagsgesellschaft Geest&Portig K.-G., Leipzig, 1978.
5. Ardenne, M. von, Tabellen zur Angewandten Physik I. Band, VEB Deutscher Verlag der Wissenschaften, Berlin, 1979.
6. Ardenne, M. von, Tabellen zur Angewandten Physik III. Band, VEB Deutscher Verlag der Wissenschaften, Berlin, 1973.
7. Swanson, L.W., Swind, G.A. and Bell, A.E., J. Appl. Phys., **51** (1980), p.3453.
8. Bell, A.E. and Swanson, L.W., Appl. Phys., **A41** (1986), p.335.
9. Taylor, G.I., Proc. Roy. Soc., **A280** (1964), p.383.
10. Swanson, L.W., Nucl. Instr. and Meth., **218** (1983), p.347.
11. Swanson, L.W., Appl. Surf. Sci., **76/77** (1994), p.80.
12. Mair, G.L.R., J. Phys. D.; Appl. Phys., **20** (1987), p.1657.
13. Komuro, M. and Kato, T., J. de Physique, **C6** (1987), p.141.
14. Henke, D. and Hentschel, R., Experimentelle Tech. der Phys., **37** (1989) 1, p.67.
15. Sakai, Y. and Katsumata, I., Jap. J. Appl. Phys., **24** (1985), p.337.
16. Papadopoulos, S., Phys. D. Appl. Phys. **21** (1988), p.194.